Photonic States and Band Structure in Non-Uniform Metal-Dielectric Photonic Crystal Organic Light Emitting Diodes

Photonic States and Band Structure in Non-Uniform Metal-Dielectric Photonic Crystal Organic Light Emitting Diodes

A Thesis Presented

by

Thomas Charles Cleary

to

The Faculty of the Graduate College

of

The University of Vermont

In Partial Fulfillment of the Requirements
for the Degree of Master of Science
Specializing in Physics

August, 2023

Defense Date: July 17th, 2023
Thesis Examination Committee:

Matthew S. White, Ph.D., Advisor
Matthew D. Liptak, Ph.D., Chairperson
Randall Headrick, Ph.D.
Cynthia J. Forehand, Ph.D., Dean of the Graduate College

Abstract

In this work, a computational approach is used to study Metal-Dielectric Photonic Crystal Organic Light Emitting Diodes (MDPC OLEDs) and the changes that non-uniform dielectric layers bring to the photonic band structure. A simplified MDPC OLED constructed from silver metal layers and light-emitting layers of Alq3 is modeled using the transfer matrix method which allows for the simulation of thousands of devices featuring a wide range of size defects in one or more dielectric layers. Three-cavity devices are simulated with aberrant cavities of sizes from 1% to 200% the standard size. Emission plots and electric field profiles are used to illustrate the effects of the defects in these cavities. The results of these simulations are described by two models, based on the coupled oscillator and perturbed harmonic mode models of MDPC OLEDs. We describe the precise control of defect states that exist in the photonic band gap, and identify the importance of the defect cavity position in determining the band structure of a device with such states. The work is expanded into devices with more cavities, and devices with multiple defects, showing how the same principles of cavity coupling can be applied to predict the behavior of arbitrarily large devices with any number of defects.

Table of Contents

List of Figures

Chapter 1

Photonic Crystals

Photonic crystals are a special class of metamaterial that transmit or reflect certain wavelengths of light based on the physical characteristics of the crystal. Alternating layers of materials with different indices of refraction create optical paths where only certain wavelengths resonate [2, 3]. Inside the crystal, the size of the unit cell determines which wavelengths interfere constructively or destructively, in a fashion directly analogous to the electronic band theory of semiconductors. [2] A photonic crystal may be structured in one, two, or three dimensions, with the simplest 1-d case requiring layers of material stacked periodically. Photonic crystals of all types can be found in nature. Some insect chitin contains wide, thin layers of material that stack to form one-dimensional photonic crystals. Thin fibers in the tails of some birds can form a lattice that acts as a two-dimensional photonic crystal. Three-dimensional photonic crystals can be found in the dust that covers butterfly wings and gives them their distinctive color patterns [4]. Unlike other sources of color, it is not the absorption spectrum of a chemical that determines which wavelengths are reflected and seen. Instead the near-wavelength scale variations in the index allow only certain wavelengths

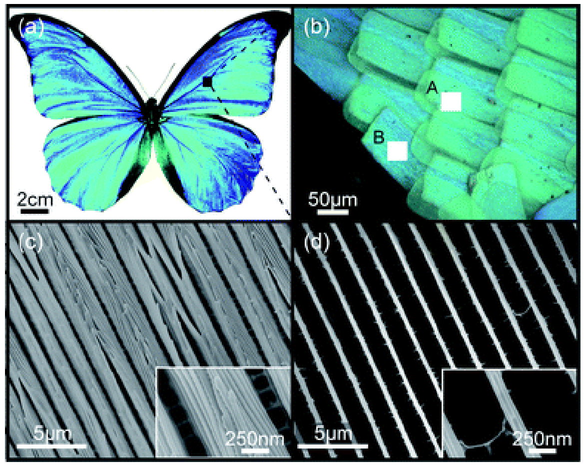

Figure 1.1: Natural Photonic Crystals in Butterfly Wings [1]

to transmit. This gives rise to the distinctive iridescent quality of natural photonic crystals. The wavelengths that are reflected off the crystal are not the same as the wavelengths that are transmitted through, and the peak transmitted wavelength will depend precisely on the angle at which it is viewed. [4, 5]

One of the earliest studied photonic crystals was the Distributed Bragg Reflector or Bragg Mirror. These are one-dimensional photonic crystals with periodic layers of dielectrics with significantly different indices of refraction. Bragg mirrors are constructed with many layers of dielectrics, creating a great number of interfaces where light may be transmitted or reflected. For a given Bragg Mirror, there will be a span of wavelengths known as a stopband that are almost entirely reflected. The width of this band depends directly on the number of layers and the difference in refractive index between the dielectrics. The mirror is designed so that each dielectric layer has the same optical path length, and peak reflection happens for a wavelength that is exactly 4 times this length. The reflection of this wavelength is driven by destructive interference within the device. The usefulness of a Bragg Mirror comes from its se-

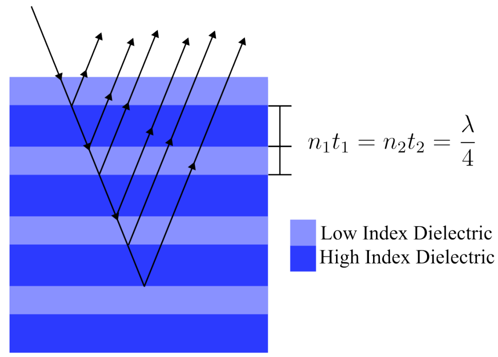

Figure 1.2: Distributed Bragg Reflector

lective reflection of certain wavelengths, so they are used in devices like lasers where wavelength purity is important.

To get a better idea of how photonic crystals function in general, let's take a close look at a Bragg Mirror. Each layer has an optical path length of one-quarter wavelength, so as light propagates through the device, the phase shifts by $\frac{\pi}{2}$ for each layer of material it passes through. There is no phase shift associated with transmitting from one layer to the next, but there is a phase shift of π if reflection happens in a transition from a low-index material to a high-index material. Using figure 1.2 as an example, a beam that reflects in this manner will have traveled through an odd number of layers on the way in, and the same number on the way out, so its phase will have shifted by $(2n-1)\pi$ by traversal and again by π for reflection, giving a net phase of $2n\pi$ for any beam that reflects off a low-index to high-index boundary and exits the device. It is equally likely for light to reflect off a high-to-low boundary as it is the low-to-high that we've already discussed. In this case, the beam will have traveled through an even number of layers before reflecting and there is no phase shift for a high-to-low index reflection, resulting in a total phase of $2n\pi$ by the time the light exits the device. The resulting outward-moving beam consists of completely coherent light, with each reflected beam interfering constructively with the others. This additive behavior leads to the result that each additional layer increases the reflectivity of the device. The approximate form of the reflection coefficient of a device in a vacuum is given by Equation 1.1 [6].

$$r = \frac{(n_2)^{2m} - (n_1)^{2m}}{(n_2)^{2m} + (n_1)^{2m}} \tag{1.1}$$

The total number of layers is given by $2m$, and n_1 and n_2 are the refractive indices of the low- and high-index materials. In this way, a device constructed with a large enough number of repeated unit cells can approach a reflectivity of 1. The width of the stop band is not controlled by the number of layers, but instead depends only on the difference in refractive index between the alternating dielectrics [6].

While the distributed Bragg reflector is only one example of a photonic crystal, it highlights many of the key features that all photonic crystals have in common. The repeating structure of the material works, along with changing refractive indices, to facilitate constructive or destructive interference of particular wavelengths of light. This interference leads to transmission bands and stop bands that depend on the energy of the photon, analogous to the conduction and valence bands in semiconductors. This analogy makes photonic crystals valuable for research into advanced integration of optical devices with electronics, including the possibility of completely optical circuits [7].

The most widely studied photonic crystals are dielectric-dielectric crystals (like the Bragg Mirror), but it is also possible to create metal-dielectric crystals whose unit cell contains both a metallic mirror and a dielectric cavity. The unit cell of a metal-dialectric crystal can be modeled as a Fabry-Pèrot resonator, a device widely

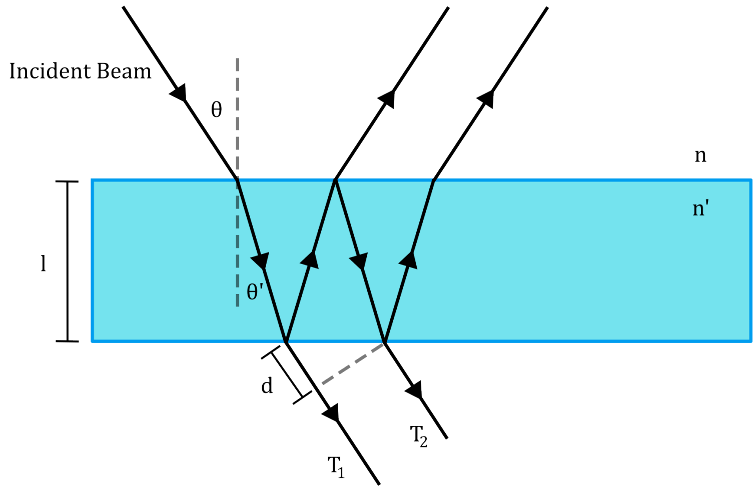

Figure 1.3: Reflection and refraction through a simple Fabry-Pèrot resonator

used in optics. It is formed by a single dielectric cavity with a thin, partially-reflective mirror on each end. Light entering a Fabry-Pèrot resonator creates standing waves in the cavity and the resonator allows transmission of wavelengths that have a node at the position of each mirror [8]. Other wavelengths interfere destructively and are almost entirely reflected. The Fabry-Pèrot etalon uses this property of the resonator to filter wavelengths of light.

Light passing through a simple Fabry-Pèrot resonator made of a single transparent layer is shown in Figure 1.3. To find the transmission from this device, one must consider each possible beam directed to the right by a series of reflections and transmissions. The first two such beams are shown in the figure. Each subsequent beam will have an additional phase shift compared to the previous beams, and the interference of these phases, combined with the reflection coefficients of the boundaries, will determine the intensity of the transmitted light. Beam T_2 will have traveled an additional distance of $\frac{2l}{\cos\theta'}$ while inside the layer, while beam T_1 will have traveled the distance d outside the layer, given by Equation 1.2.

$$d = 2l \tan\theta' \sin\theta \tag{1.2}$$

$$\Delta S = \frac{2n'l}{\cos\theta'} - 2nl \tan\theta' \sin\theta \tag{1.3}$$

The difference in optical path length for the two beams is given by Equation 1.3. After applying Snell's Law to account for the difference in angles and indices of refraction, the phase shift between the beams can be determined by Equation 1.4.

$$\delta = 2n'l \sin\theta' \tag{1.4}$$

The ratio of amplitudes of transmitted light to incident light can be found by the infinite series that accounts for both the decreasing amplitude and phase shift of each subsequent beam.

$$\frac{A_t}{A_i} = t^2 \sum_{n=0}^{\infty} r^{2n} e^{in\delta} = \frac{t^2}{1 - r^2 e^{i\delta}} \tag{1.5}$$

The square of this value determines the transmissivity of the device as a whole, for a particular wavelength.

$$T_{device} = \frac{(1-R)^2}{1 - 2R\cos\delta + R^2} \tag{1.6}$$

This equation generates the Airy distribution, and is a well known result in optics. Figure 1.4 shows the transmissivity of a simple Fabry-Pèrot resonator. Each curve represents a device with a reflectivity on its boundaries. More reflective boundaries lead to more narrow peaks and broader stopgaps. As expected, the transmission is at a maximum when the phase shift is a multiple of 2π. In the specific, but useful, case of normal incidence, the result is that the most highly transmitted wavelengths

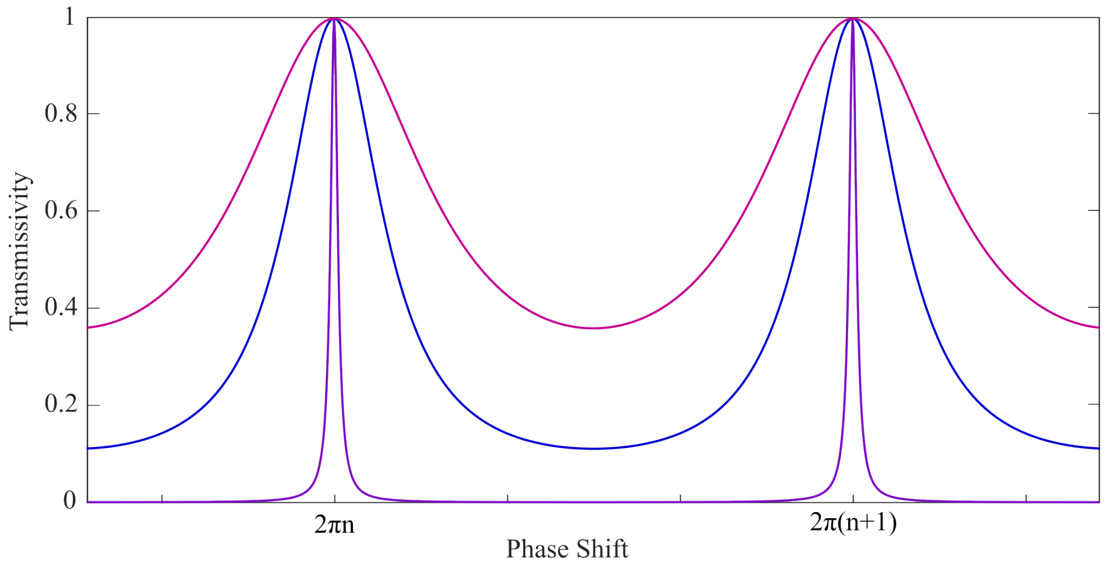

Figure 1.4: The Airy Distribution for Fabry-Pèrot resonators with R = 0.25, 0.5, 0.95 respectively, descending

are exactly those that can form standing waves with a node at each boundary.

$$m\frac{\lambda}{2} = n'l \tag{1.7}$$

Metal-Dielectric Photonic Crystals (MDPCs) are not as restrictive as Fabry-Pèrot resonators in their transmission profiles. MDPCs with many periods exhibit broad stop bands and multi-peaked transmission bands, similar to their dielectric-dielectric counterparts [9]. MDPCs are of particular interest because any electrically driven optical device could incorporate metal electrodes into the optical stack. An example of such a device is a MDPC Organic Light Emitting Diode (OLED), where the voltage across the electrodes drives electroluminescence in a carefully chosen dielectric material. [10] In such a device, the dielectric layers act as both emitters and resonant cavities. The distinctive properties of OLEDs have led to their widespread study and application, but the MDPC OLED class remain in their nascency.

Chapter 2

Organic Light Emitting Diodes

Light emitting diodes (LEDs) are a dominant source of light in modern life, particularly with regards to small-scale applications like electronics. LEDs provide a narrow spectrum of bright light that can be emitted from a very small source. In a traditional LED, voltage applied across a semiconductor facilitates electron-hole recombination emitting photons whose energy depends on the energy gap between the valence and conduction bands. LEDs made with electroluminescent organic compounds have been shown to have some significant advantages over their traditional counterparts.

Organic LEDs (OLEDs) function in largely the same manner as conventional LEDs. Electrons and holes that are injected into the organic compound recombine to emit photons at particular frequencies. OLEDs are constructed in a multi-layer stack, with the emission layer sandwiched between the anode and the cathode and often some other functional layers that facilitate selective transport of electrons and holes [11]. This simple structure allows OLEDs to be made in wide, flat sheets, and requires one or both of the electrodes to be transparent, so that emission can be viewed through the top of the stack. The simplicity of the design, along with the use of a wide selection of possible light-emitting organics allows for some novel applications. Of particular interest is the fact that organic emitters need not be stiff crystals like their inorganic counterparts, allowing for the design and creation of flexible or transparent displays [11, 12]. Along with the advancements that have been made, OLEDs have brought a host of new challenges.

In their modern form, most OLEDs have taken on a few additional components to address the technical challenges they face. The applied voltage across the electrodes must be great enough to excite electrons and holes to the conduction band, allowing them to travel from the electrodes to recombine in the emissive layer. This voltage

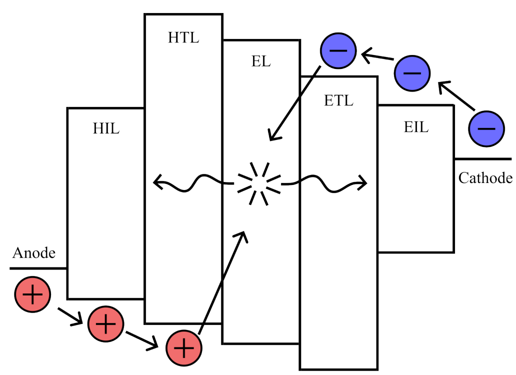

Figure 2.1: Light Emission in multi-layer OLED

requirement depends on the band gap of the emitter and the alignment of the work functions of the anode and cathode with the highest-occupied and lowest-unoccupied molecular orbital levels of the emitter. To reduce the required voltage, injection layers can be used directly adjacent to the electrodes [13, 14]. The injection layer is specially designed for the easy excitation of electrons or holes on the interface with the electrode. Another challenge is that organics with desirable emission may not transport electrons and holes at the same rate. A difference in transport speed can cause recombination to occur far from the center of the device in zones that are too close to one electrode or the other to generate ideal emission patterns. In extreme cases, recombination can occur in injection layers which have completely different emission properties than the desired emission layer. To correct for this possibility, transport layers lie between injection and emission materials, ensuring that recombination happens in the correct physical location [8].

When electrons and holes recombine, they form short-lived bound states called excitons. An exciton is a neutral quasi-particle formed by an electron and a hole in mutual orbit. Dynamically, the behavior of an exciton is akin to a hydrogen atom, with the coulomb attraction between the electron and hole providing the binding energy for the particle. The collapse of these particles is responsible for the emission of light, so their behavior is a crucial part of understanding OLEDs. Their binding energy depends on the relative permittivity of the material in which they form because the coulomb attraction is reduced by screening from nearby electrons [15]. Additionally, the semiconductor band structure determines the effective mass of the electron and the hole, which also affect the binding energy. These effects lead to the result that the binding energy, and therefore the frequency of emitted photons, depend very finely on the electron structure of the material, explaining why similar organics may have drastically different emission spectra [16].

In the scheme described above, the emission of the device depends almost entirely on the emission spectrum of the emissive material. Different materials are used for the purpose of changing the peak wavelength or the spectral width of the emission. For example, in a screen on a digital device, three distinct organic semiconductor emitter materials must be used to create the red, green, and blue pixels. None of these

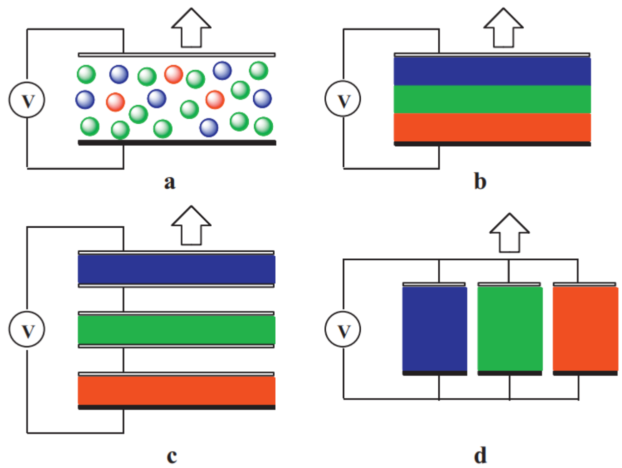

Figure 2.2: Reproduced from Zhou, et. al. General approaches to generate white light from OLEDs using multiple emitters. (a) Single-EML structure, (b) multilayer EML structure, (c) stacking and tandem structure and (d) striped structure.

would be suitable for use in a solid-state lighting device alone, which would require either one single material that emits a broad-spectrum white light or a combination of monochromatic emitters. Broadband, white-emitting organic semiconductors have proved very difficult to find, so most advances in the production of white OLEDs have come from combining materials with red, green, and blue emissive properties, as shown in Figure 2.2 [17]. Many materials with desirable emission spectra have been identified and applied. One example is Tris(8-hydroxyquinoline)aluminum(III) or Alq3, which emits a relatively broad spectrum of light, mostly surrounding green frequencies. The free-space emission profile of Alq3 is shown in Figure 2.3. Exactly which properties are considered desirable depends on the application in which they are being used.

The emission spectrum of Alq3 (or any other electroluminescent organic) can be modified by combining the ideas of an OLED with those of a photonic crystal. Replacement of the transparent mirrors with mirrors that are more reflective turns our

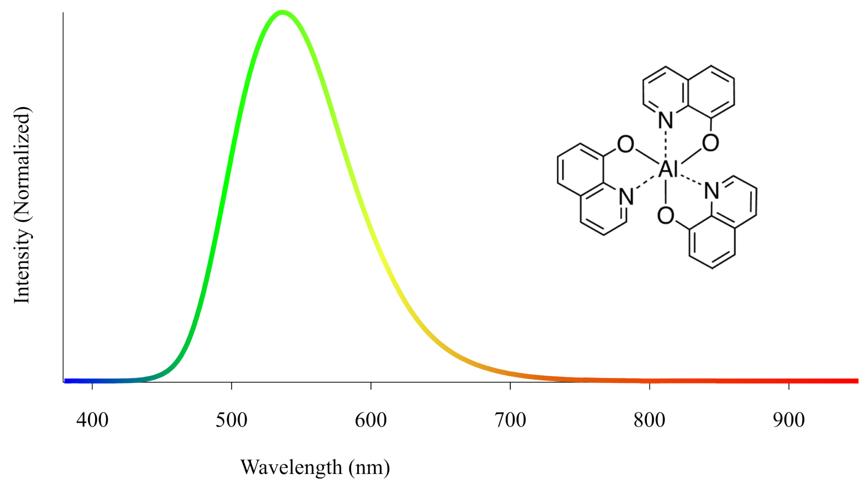

Figure 2.3: Emission Spectrum of Alq3

simple OLED into a Fabry-Pèrot resonator with a luminescent cavity. Such a device is known as a microcavity OLED. The emission of a microcavity OLED depends on both the emissive properties of its emission layer and the physical parameters of the cavity itself. The microcavity affects the peak wavelength, intensity, polarization, linewidth, and directionality of the emission [8,18,19]. A primary benefit provided by microcavity OLEDs is that they allow the control of peak wavelength and linewidth without changing the emissive material. Stacked microcavities create bands of emission peaks, which are offer entirely new avenues for emission control.

Chapter 3

Photonic OLEDs

3.1 Microcavity OLEDs

The marriage of OLEDs and Photonic Crystals results in a light-emitting device whose characteristics depend heavily on both the electroluminescence of the the organics and the physical parameters of the device. Such devices are constructed by replacing the mostly-transparent mirrors of an industry-standard OLED with highly reflective mirrors that turn the organic layers into a resonant cavity [8]. Mirrors with high reflectivity can be made from thick layers of highly conductive metals, or they can follow a distributed Bragg reflector design as outlined in Chapter 1. Sufficiently reflective mirrors are capable of suppressing any broadband emission that may be characteristic of a given organic, but peak emission for a given wavelength is still limited by the free-space emission of the organic. It remains impossible to generate a peak where the organic does not emit at all. Microcavity OLEDs have been found to be effective in peak narrowing, color selection, and improving efficiency [8, 20].

Figure 3.1 shows how the peak wavelength of the emission of Alq3 can be controlled

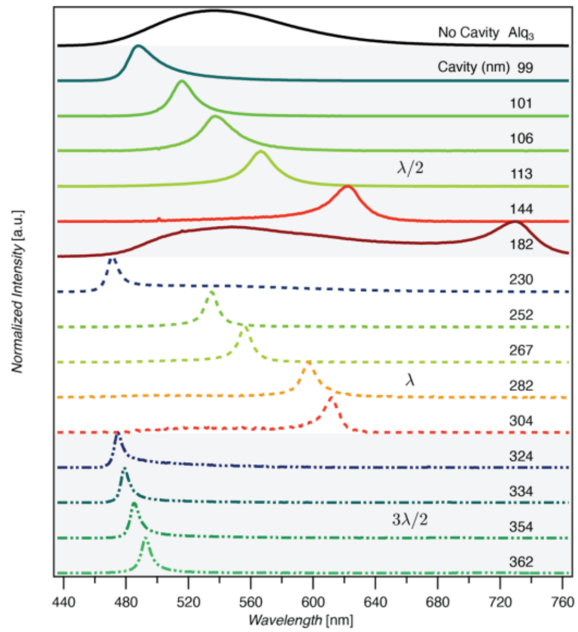

Figure 3.1: Emission from microcavity OLEDs of varying sizes (reproduced from Dahal, et. al. 2021)

by changing the optical path length of the cavity. When viewing normal emission, the peak wavelength should be that with an anti-node at each mirror as described in Equation 1.7. This state is described as the $\frac{\lambda}{2}$ state because the cavity size is half of the wavelength. The full range of harmonics are theoretically present, but Alq3 emits almost exclusively in the visible range, so the λ and $\frac{3\lambda}{2}$ states can only be measured if the cavity size is increased to the point that those wavelengths fall between 400 and 800 nm.

For a single cavity, the resonance condition depends on the cavity size and the penetration depth in the mirrors. It can be expressed as [19]:

$$\lambda_j = \frac{2}{\left[j - 2\left|\frac{\phi^{\uparrow}+\phi^{\downarrow}}{4\pi}\right|\right]} \sum_i n_i t_i \qquad j = 1, 2, 3, \ldots \tag{3.1}$$

Where, $\phi^{\uparrow}$ and $\phi^{\downarrow}$ are the phase shifts at each mirror, n_i and t_i represent the index of refraction and thickness of the active layers between mirrors, and $L = \sum_i n_i t_i$ is the optical path length of the combined organic layers.

The phase shift ϕ is depends on the optical properties of the organic and metal layers [19]:

$$\phi = \arctan[\frac{n_{\mathrm{org}}\, k_{\mathrm{m}}}{n_{\mathrm{org}}^2 - n_{\mathrm{m}}^2 - k_{\mathrm{m}}^2}] \tag{3.2}$$

Here n_{m} and k_{m} are the real and imaginary parts of the index of refraction of the mirrors and n_{org} represents the index of refraction for the organic layer. While there is some variation, many of the organic semiconductors have $n \approx 1.7 - 1.8$ and can be approximated as a homogeneous material to first order. We assume that the organics are lossless, so the imaginary part of the organic's index of refraction is zero.

The resonant wavelength is directly proportional to the optical path length, which is exactly the property that allows us such fine control over the emission of the device. The agreement between the theory provided by Equation 3.1 and experiment is shown in Figure 3.2.

In a microcavity OLED, it is possible for the properties of an emission peak to depend on the reflective properties of the mirrors to a greater extent than would be predicted by the equations that describe the behavior of Fabry-Pèrot resonators. This effect is caused by the interaction between the standing wave states of light in the cavity with the excitons that form in the emitting layer [18, 21]. The coupling of these two phenomena leads to a new quasiparticle referred to as exciton-polaritons, or simply polaritons. Higher levels of reflection from the mirrors lead to more intense standing waves within the device, which in turn causes a greater coupling. The stand-

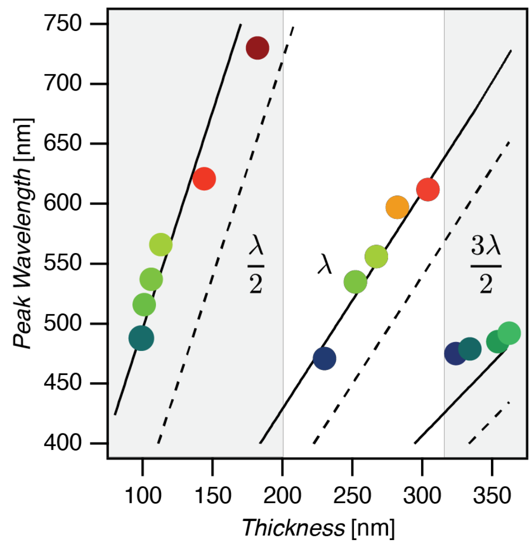

Figure 3.2: Experimental and theoretical peak emission for cavities of different sizes. Dashed lines calculate peak emission without taking penetration into the mirrors into account. Solid lines represent Equation 3.1. (reproduced from Dahal, et. al. 2021)

ing waves span the entire cavity, which gives the polariton a much larger physical size than an exciton alone. Spatially extended polaritons can interact with each other in ways that are not possible for individual excitons, leading to a greater level of coherence and therefor a smaller range of binding and emission energies [18]. Polaritons can reasonably be said to exist in the strong-coupling regime of microcavity devices, which involves thick mirrors with very high reflectivities. Devices with relatively thin mirrors are not well-described by the presence of polaritons and are said to be in the weak-coupling regime.

3.2 Metal-Dielectric Photonic Crystal OLEDs

More complex photonic OLEDs can be formed by creating a one-dimensional photonic crystal using the single microcavity OLED as a unit cell. The mirrors in such a design double as electrodes, making this device necessarily a metal-dielectric photonic crystal. The sharing of electrodes among adjacent cavities requires that each cavity be oriented opposite of the cavities on either side. Generally, this produces a crystal whose unit cell is constructed of two cavities, one with each orientation. [10] However, OLED design can be adjusted to increase the symmetry of the device, effectively shifting the unit cell back to a single microcavity. [22] Such devices are generally known as Metal-Dielectric Photonic Crystal (MDPC) OLEDs.

Given that each unit cell has the same resonance condition, one might expect that the emission would feature stronger, more steeply peaked emission at the wavelength described by the resonant condition, but this is not what is observed. Instead, the resonant modes couple together, creating new emission peaks. The interaction between two coupled microcavities is analogous to coupled oscillators in classical mechanics, but the best language for it comes from quantum mechanics. The two states that emerge from the two-cavity device can be viewed as bonding and anti-bonding states - one with slightly higher energy and one with lower energy. Larger crystals have rich photonic band structure where each of the microcavity states described by Eq. 3.1 form a band with the number of emission peaks equal to the number of cavities in their structure.

For MDPC OLEDs, the emission can be described as an intermediate stage between two natural extremes. The first extreme is the case where the internal metallic mirrors become infinitely thin, and thus lose their reflectivity. In this case, the entire device acts as a single extended cavity. The second extreme is where the cavities are separated by such thick mirrors that there is no interaction between them, and they do not couple at all. In this case, each cavity produces the same emission as all the others.

Beginning from the thin-mirror, extended-cavity case, we can explain the behavior of the states using a perturbation model. The introduction of the mirrors perturbs the standing wave electric fields in the extended cavity because the conductivity of the metal layers allows charges to move, reducing the strength of the electric field. This leads to the effect that metallic mirrors tend to enforce nodes at their positions. For a two-cavity device, only one mirror is introduced, in the very center of the extended cavity. While this mirror will greatly disrupt the fundamental mode and the third harmonic, it has a much smaller perturbative effect on the second and fourth harmonics, which already have nodes at the mirror's location. The perturbation of a given mode is directly correlated to the increase in the energy of that state [10]. In this way, for a two cavity device, each of the odd harmonics sees a large increase in its energy, while the even harmonics see only a small increase in energy. This effect leads to the formation of photonic bands and band gaps. For the two-cavity device, bands of two states will form. The first harmonic will be close in energy to the second harmonic, and the third harmonic will be close to the fourth. Between these bands, there are gaps larger than the unperturbed state spacing where no states are present.

Since the level of perturbation depends on the alignment of mirrors with existing

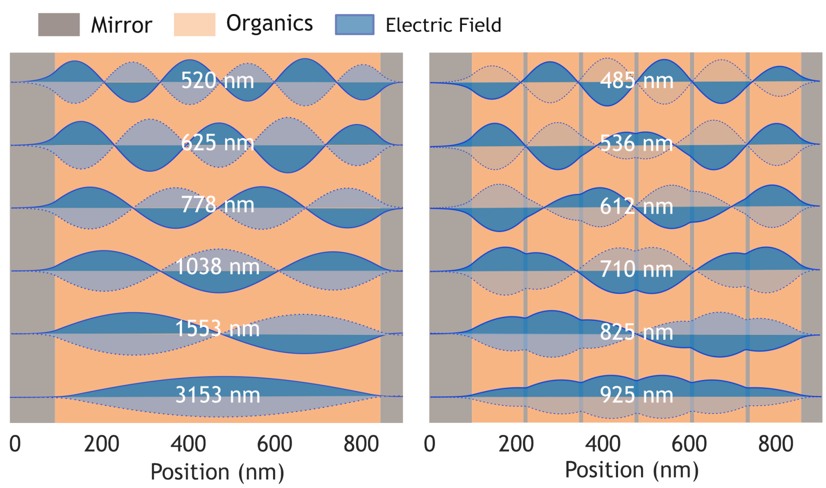

Figure 3.3: Perturbation of extended cavity states by introduction of thin metallic mirrors (reproduced from Allemeier, et. al. 2021)

nodes in the standing electromagnetic waves, the number of cavities determines which states experience the least perturbation. The harmonic of the same number as the number of cavities will always be the least perturbed, and so will always be highest energy state in the first band of states. The harmonic exactly one level higher will have antinodes at exactly the mirror positions, so it will always experience great perturbation and therefore its energy shift will create the band gap and it will be the lowest-energy state in the second band. For an N-cavity device, then, bands will be formed with N states. As mirror thickness increases, the states are further perturbed, and so state spacing decreases, bands narrow, and band gaps widen. As this happens, we approach the thick-mirror extreme and the extended-cavity harmonics become degenerate [10].

The same behavior can be described from the opposite extreme. In the case where mirrors are extremely thick, electromagnetic radiation created in one cavity

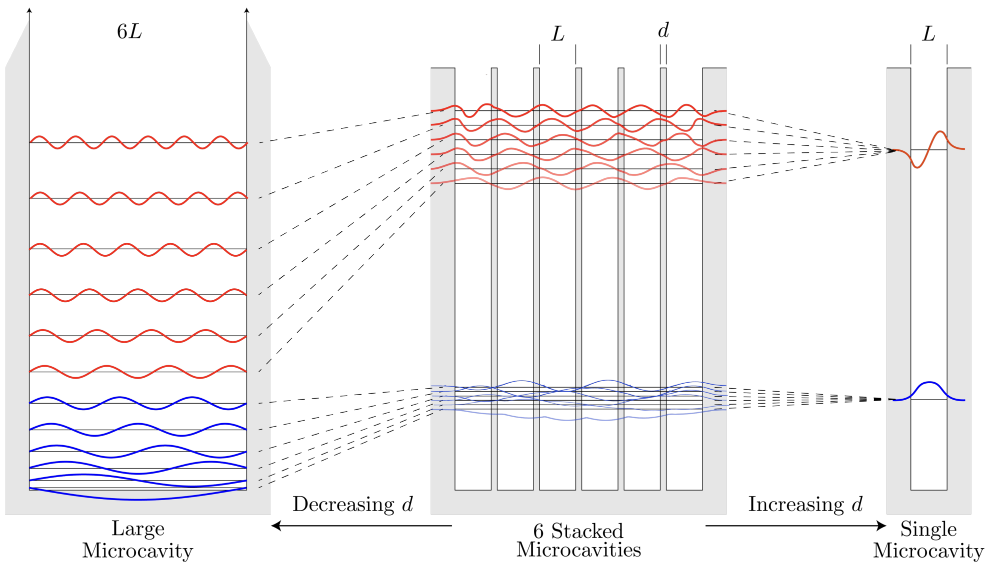

Figure 3.4: Formation of Photonic Bands from two extremes (reproduced from Allemeier, et. al. 2021)

scarcely reaches adjacent cavities, and each cavity is isolated from its neighbors. Free of any external influence, the emission of each cavity will depend only on its physical parameters. Since the cavities are identical, each of these isolated cavities will generate identical emission spectra as well [8]. As the mirrors get thinner, the states begin to couple and split. In an N-cavity device, each individual state becomes N distinct states in a band, loosely centered on the energy of isolated, single-cavity states that generated them [10]. Figure 3.4 shows how these two extremes meet in the middle to form the band structures that are characteristic of MDPC OLEDs.

Chapter 4

Transfer Matrix Simulation

The transfer matrix model is an accurate and efficient tool for representing the electric field inside a one-dimensional optical device. This simulation relies on linear algebra, which computer software can handle quickly and easily, allowing complicated analysis to be done in a short amount of time on any machine. The model is also rigorous enough to allow investigation into a wide array of properties for a given optical device.

The transfer matrix follows a mathematical formalism in which the electric field at any position is described by a complex 2-vector. The two components of the vector describe leftward- and rightward-travelling electromagnetic waves. Matrices are used to manipulate these vectors to describe the behavior of the EM waves at any other position. The matrix that allows for comparison between two sides of an optical device is called the Transfer Matrix. The transfer matrix is created by matrix multiplication of propagation matrices for each bulk material that the EM waves must propagate through, as well as scattering matrices that describe the reflections and transmissions at each material interface within the device.

The scattering matrices are defined by the Fresnel equations which describe the behavior of electric field waves at the boundary between two dielectric materials. The s- and p-polarizations are treated separately, as the behavior of each polarization will be different for any light with non-normal incidence. The complex amplitude reflection coefficients (r_s and r_p) describe the ratio of the complex amplitude of the incident electric field with the complex amplitude of the reflected electric field. The reflectivity (R) is given by the square of the complex amplitude reflection coefficient, and refers instead to the ratio of reflected power.

$$\begin{aligned} r_s &= \frac{n_1 \cos\theta_i - n_2 \cos\theta_t}{n_1 \cos\theta_i + n_2 \cos\theta_t} \\ r_p &= \frac{n_2 \cos\theta_i - n_1 \cos\theta_t}{n_2 \cos\theta_i + n_1 \cos\theta_t} \end{aligned} \tag{4.1}$$

In these equations, n_1 and n_2 are the complex indices of refraction for each material. Using the complex index of refraction allows us to consider the absorption of light by the material as well as the propagation characteristics. The angles of incidence and transmission are related to each other through Snell's Law, Equation 4.2.

$$n_1 \sin\theta_i = n_2 \sin\theta_t \tag{4.2}$$

In these equations, the complex amplitude transmission coefficients (t_s and t_p) are defined such that the total amplitude of reflected and transmitted waves is equal to the amplitude of the incident wave, provided that the imaginary part of both indices of refraction are zero. They are given in Equation 4.3.

$$
\begin{aligned}
r_s &= \frac{2n_1 \cos\theta_i}{n_1 \cos\theta_i + n_2 \cos\theta_t} \\
r_p &= \frac{2n_1 \cos\theta_i}{n_2 \cos\theta_i + n_1 \cos\theta_t}
\end{aligned}
\tag{4.3}
$$

Sign conventions dictate that $t_s - r_s = 1$. The p-polarizations have the relation $\frac{n_2}{n_1} t_p - r_p = 1$. Likewise, while the reflected beams, which remain in the same medium, have the simple relation $R = |r|^2$, while the transmitted beams will be traveling at different angles and speeds, requiring $T = \frac{n_2 \cos\theta_t}{n_1 \cos\theta_i} |t|^2$. These complex amplitude coefficients allow us to construct our scattering matrix for each interface. The scattering matrix acts on the electric field vector in medium 1 and produce a vector describing the electric field in medium 2. The calculation shown in Equation 4.4 must be performed separately for the s- and p-polarizations at each interface.

$$
\vec{E}_1 = \frac{1}{t} \begin{bmatrix} 1 & r \\ r & 1 \end{bmatrix} \vec{E}_2 = \boldsymbol{M_{1,2}} \vec{E}_2 \tag{4.4}
$$

The propagation matrices are constructed much more easily, and they are identical for the two polarizations. A wave that has traveled a distance x through a medium with complex index of refraction n will have the form $E = e^{ikx} E_0$ compared to its initial state E_0, where k is the wave vector $k = \frac{\omega}{c} n$. For a wave travelling at an angle θ to the normal, this propagation becomes $E = e^{ikx \cos\theta} E_0$. Equation 4.5 turns this relationship into a propagation matrix for the left- and right-travelling waves.

$$\vec{E_1} = \frac{1}{t}\begin{bmatrix} e^{ikx\cos\theta} & 0 \\ 0 & e^{-ikx\cos\theta} \end{bmatrix}\vec{E_0} = \boldsymbol{D}\vec{E_0} \tag{4.5}$$

These two matrices constitute everything that is necessary to describe transmission of an electric field through a one-dimensional optical device. The electric field on the far-left can be related to the electric field on the far-right by the transfer matrix, shown in Equation 4.6.

$$\vec{E_L} = \boldsymbol{M_{L,1}D_1M_{1,2}D_2M_{2,3}}...\boldsymbol{D_nM_{n,R}}\vec{E_R} = \boldsymbol{S}\vec{E_R} \tag{4.6}$$

The simplest calculation we can perform with the transfer matrix is to calculate the emitted and reflected amplitudes when a monochromatic light is shone normal to a one-dimensional (but many-layered) optical device. After constructing the transfer matrix based on the wavelength of light and optical properties of each layer, we suppose the light is being shone in from the left. This allows us to set the electric field on the right side of the device to $\vec{E_R} = \left[\begin{smallmatrix}1\\0\end{smallmatrix}\right]$ because we know that there will be no left-moving waves on the right side of the device. The only electric field there will be the transmitted right-moving waves from the incident light. After calculating $\vec{E_L}$, we can normalize to its right-moving part, which represents the incident beam. The left-moving part of $\vec{E_L}$ gives us the reflected beam, and the normalized right-moving part of $\vec{E_R}$ provides the transmitted beam. These two amplitudes may not be related to each other in any obvious way, because our transfer matrix allows for absorption in the device. It is worth noting that we could not have performed this calculation by starting with our known incident beam, because $\vec{E_L}$ contains both the known incident part, and an unknown reflected part.

Having calculated the entire electric field on both sides of the device, we can use our scattering and propagation matrices to propagate the external electric field inside the device, and in this way, we can calculate the behavior of the electric field at any point inside the device. This allows us to construct a profile of the electric field within the device, which is useful for visualizing standing wave states that may exist inside the device at certain wavelengths. The transfer matrix method also allows us the flexibility to solve for the emission from a device that has electrically active electroluminescent layers.

When designing the simulation to handle electroluminescent layers, it is important to identify the positions at which light will be generated. Electroluminescent materials are chosen for the spectra of light that they produce, and as such, do not always have the most desirable electrical properties. It is often the case that a the electroluminescent layer is a much better transporter of either holes or electrons than the other. This will result in most recombination occurring very close to the boundary between the electroluminescent layer and the adjacent transport or injection layer. The most commonly used materials have been tested extensively, so there is data available to describe the probability distribution of recombination sites. This data can be used to generate sources within the transfer matrix.

Light sources are points of discontinuity within the transfer matrix model. As electromagnetic waves pass a source point, the amplitude is instantaneously increased by an amount dependent on the recombination distribution and the emissive properties of the medium at that wavelength. With these properties, we can generate the source field, $\vec{A}$, a vector describing the field created at any given source position. Propagating from the source position to the external fields, we arrive at Equations 4.7 and 4.8. The half-transfer matrix from 4.8 will be inverted due to our convention for constructing transfer matrices. Our calculation in this case is simplified by the fact that, as we are only considering emission, $\vec{E_L}$ has no right-moving part and $\vec{E_R}$ has no left-moving part.

$$\vec{E_L} = \boldsymbol{S_{L \to A}} \vec{A} \tag{4.7}$$

$$\vec{E_R} = (\boldsymbol{S_{A \to R}})^{-1} \vec{A} \tag{4.8}$$

In order to find the emission from a complex device, we must construct the entire transfer matrix, but also the two half-transfer matrices for each source point. Then, we can find the emission from each source term, which must be handled separately for each polarization. Finally, we can combine all the emitted light to find the total emission profile of the device. The calculations required to find the emission profile of complex devices with many source layers take only seconds on a modern computer, giving us the power to model hundreds of devices in the span of minutes. Our research group uses this simulation extensively because it has consistently been able to predict the number and location of emission peaks in electroluminescent devices of all kinds.

Chapter 5

Emission Peaks in the Band Gap

Previous work has demonstrated the value of MDPC OLEDs for their ability to produce sharp, narrow emission peaks and the precise control they allow over the band structure. Adjustments to MDPC OLED design can change the number of states in each band, the state spacing within the band, the band location, and the size of the band gap. Any of these parameters can be designed for, but they all follow the same structure - bands of states separated by broad band gaps. A different approach must be used to position states within the band gap.

This question led us to our initial investigation of defect cavities in an MDPC OLED device. Since the band positions are based on the wavelength of the single cavity states, it stands to reason that changing the width of a single cavity within the device would create a state with a different resonance condition, that could exist in the band gap. We explored this using the transfer matrix simulation and created Figure 5.1. This figure demonstrates the simplest level of control over emission peaks in the band gap. To create this figure, we simulated six devices, each with the center cavity larger than the last, on increments of three percent.

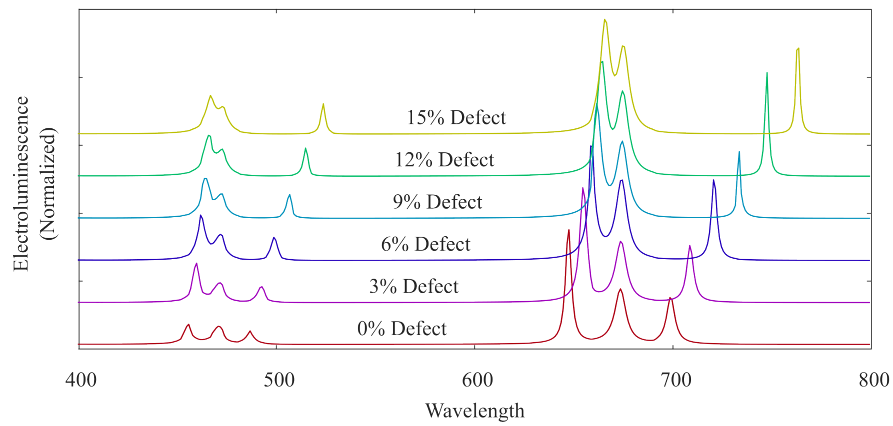

Figure 5.1: Normal Emission from three-cavity device with center cavity larger than top and bottom cavity.

5.1 Parameters

When investigating MDPC OLED devices with defect cavities, there are a number of features that are desirable to be able to explore in the emission spectrum. Since the defect cavity causes a state from the photonic band to be moved into the band gap, a clear picture would allow us to see the entire band gap, which means having two bands in the emission window of 400 to 800nm. The best way to provide this view is to use cavities that are large enough that the second and third bands fall between 400 and 800nm. The cavities in Figure 5.1 are 350 nm, with 30 nm mirrors separating them and the visible bands are the second and third band. While these devices would be difficult to manufacture, they do the best job of allowing us to observe the fundamental phenomena at play.

A number of simplifications were made to the device design in order to remove any asymmetries that might obfuscate the most basic features of the emission. Instead of the typical five-layer organic cavity, the devices used in our simulations have a single layer of Alq3. The metallic mirrors, which double as electrodes, are often made of composite materials to meet the requirements of being both an optical and electrical element. For the same reason, the cathode and anode are rarely made of the same material. In our simulation, all mirrors are made of silver.

In our early simulations, we also sought symmetry in our defects. It seemed the most natural to place the defect cavity in the center of the device, with an equal number of cavities on each side. The smallest possible device of this structure is the three-cavity device, and we found that this design highlights many of the key phenomena at play. We also fix the cavity size of the cavities without defects. This means that the overall size of our device changes depending on the size of the defect. We have found that this is a better method for exploring the defect space because the resonance condition two of the static cavities remains unchanged, regardless of the defect size.

5.2 Defect States and Their Behavior

Figure 5.1 exhibits a number of features that warrant further exploration. Most obviously, there is a state that is ejected from the band, even at very small levels of defect, and it appears to travel further into the band gap as the magnitude of the defect increases. There also appears to be a sharpening of this peak - the greater the defect, the taller and more narrow this state becomes. From this point, it feels natural to describe this travelling state as the “defect state.” We will similarly adopt the name “band states” for the emission peaks that do not leave the photonic band upon introduction of the defect. Figure 5.1 shows that these states still feel some

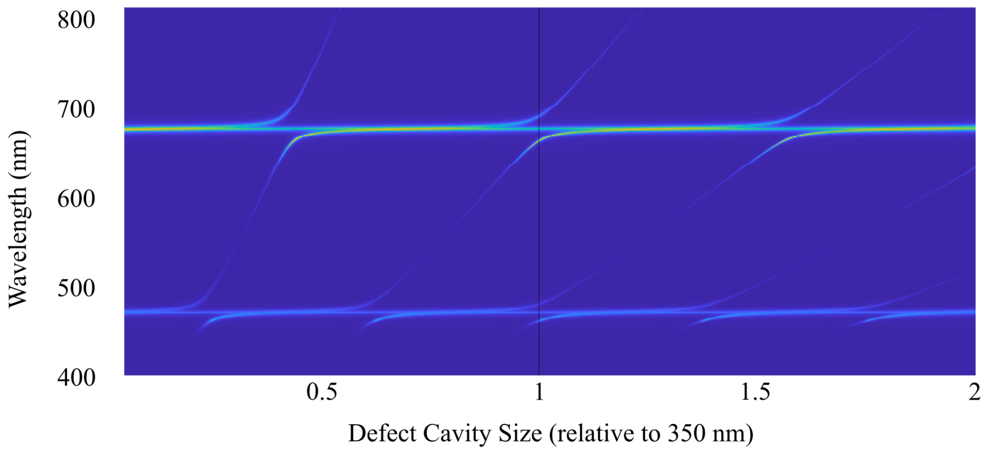

Figure 5.2: Emission from devices with a wide range of defects on the center cavity. Vertical black line at the center indicates the symmetrical MDPC OLED device with all cavities the same size. Defect cavity size is represented as a fraction of 350 nm.

effects of the defect. The spacing between the static states in the bands decreases to the point where, by 15% Defect, the two states have nearly merged, especially in the third band.

Considering the way in which the band seems to collapse when the defect state is ejected, it is natural to wonder how it will be affected when the defect state from the next band reaches it. To explore this idea, we need a much broader range of defects. We have found that all defect state behavior can be seen between defects of -100% and +100%. This means that we are considering devices from the extreme where the center cavity has no size and then growing the center cavity until it is twice the size of the other cavities. The results of these simulations are shown in Figure 5.2.

When a shorter wavelength state increases in wavelength to the point where it reaches a photonic band, it appears to cause the ejection of the highest wavelength state in that band. In this way, the defect state becomes part of the band and a

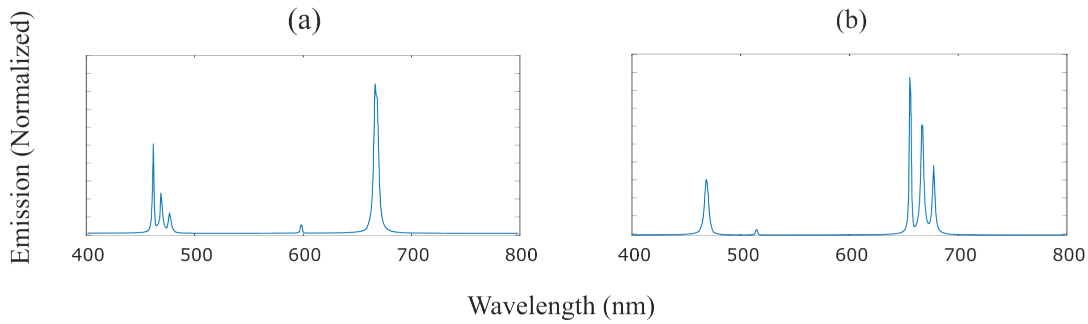

Figure 5.3: Emission from devices with one band in a perfect crystal phase. Defect cavity is (a) 1.38 and (b)1.56 times larger than the standard cavity size (350nm)

new defect state is created. As the defect is increased indefinitely, shorter wavelength states rise from the infinite number of short-wavelength bands and replace longer wavelength states in their photonic bands. Each photonic band is maintained, but states that are ejected from the fundamental band increase in wavelength without bound, as there are no further bands to interact with.

An interesting feature of this graph is the way in which the anti-crossing that is observed around the symmetrical device is recreated at various points in both visible bands. As the old defect state joins a band and ejects a new defect state, there is a defect size for which the band has the even state-spacing characteristic of a perfect crystal. However, this does not happen at the same defect size for the second and third band. Figure 5.3 highlights two devices with (a) the third band and (b) the second band exhibiting the emission of a perfect crystal. In each case, while one band has recovered its even state spacing, the other remains collapsed with a defect state having been completely ejected.

Based on these observations, the defect states appear to have two main modes of behavior. When the defect state is far from a photonic band, it's wavelength grows linearly with defect size. When the defect is near a photonic band, we observe an anti-crossing where one defect state joins the band and another is ejected.

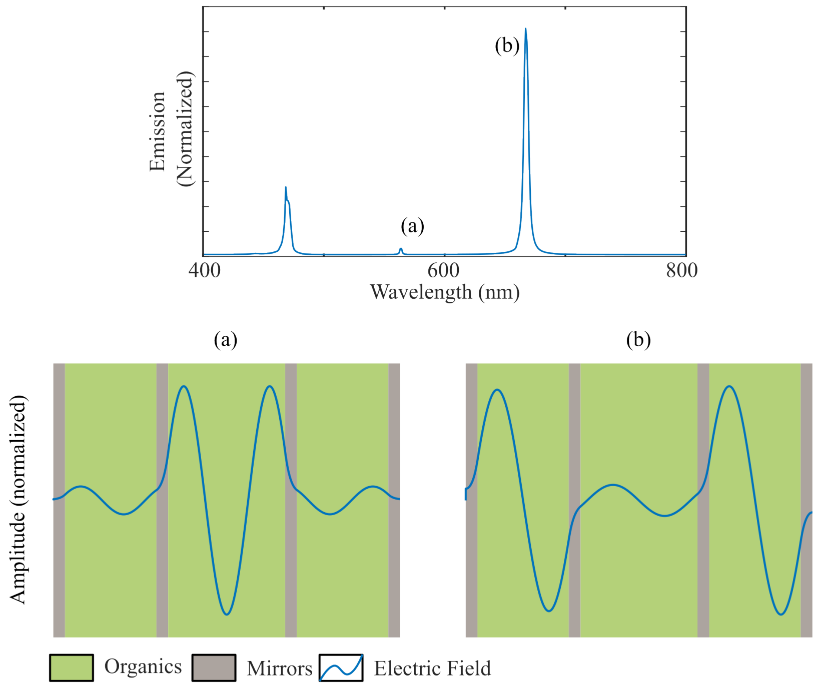

Figure 5.4: (a) Electric field profile of the defect state between the second and third photonic bands in a device with center cavity 1.28 times larger than standard cavity size (350nm). (b) Field profile for the states of the second band of the same device. Profiles of the two peaks are nearly identical, so only one is shown.

The linear increase of the wavelength of a defect state with defect size seems natural given that longer wavelengths resonate in larger cavities for any standing-wave situation. The electric field profile for a defect state in this range indicates that the defect state may act like a single-cavity state because it is almost completely confined to the defect cavity of the device. Similarly, the band states have very little intensity in the defect state. This gives our description of a "defect state" stronger meaning: it is the state that travels between bands, but it is also the state that exists within the defect cavity. The theory for the peak position of single cavities

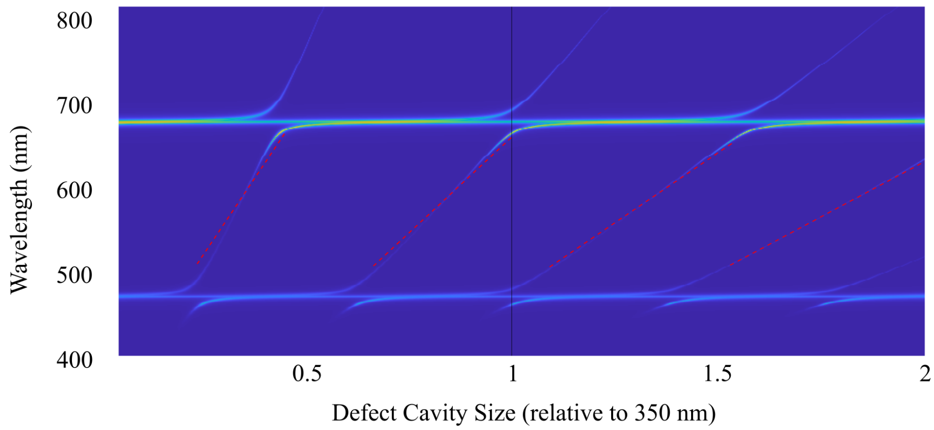

Figure 5.5: Emission from three cavity devices with central defect. Red dashed lines show slopes predicted by Equation 3.1.

is established by Equation 3.1. Based on the electric field profile in Figure 5.4, we expect this particular state follow Equation 3.1 with $j = 3$.

Figure 5.5 shows how the trajectories of the defect states compare to the slopes predicted by Equation 3.1 for $j = 1, 2, 3, 4$. The alignment of theory and simulation confirms that while far from any photonic band, the defect state acts as a completely isolated single-cavity state. It is clear that this behavior falls apart near any photonic band. While the behavior of the bands is a little more complicated, it can still be said that the two states do not deviate far from what is predicted by Equation 3.1 with $j = 2$ for the second band and $j = 3$ for the third band. Based on this, we should be able to work out a rudimentary model for predicting the locations of anti-crossings.

In our devices, all mirrors are symmetrical, and organics consist of a single layer of Alq3, allowing the following simplification to Equation 3.1.

$$\lambda_j = \frac{2}{[j - \phi/\pi]} n_{org} t_{org} \qquad j = 1, 2, 3, \ldots \tag{5.1}$$

We can predict the location of our relatively static band of states based on the static cavity thickness t_s.

$$\lambda_j = \frac{2}{[j - \phi/\pi]} n_{org} t_s \qquad j = 1, 2, 3, \ldots \tag{5.2}$$

The defect states can be located as well, according to the size of the defect cavity, t_d.

$$\lambda_m = \frac{2}{[m - \phi/\pi]} n_{org} t_d \qquad m = 1, 2, 3, \ldots \tag{5.3}$$

To find the locations of the anti-crossings, we seek the defect cavity thickness where the peak wavelength of the defect state will be close to that of the band states, which is to say, $\lambda_j = \lambda_m$.

$$t_d = \frac{(m - \phi/\pi)}{(j - \phi/\pi)} t_s \tag{5.4}$$

In this equation, the value j describes which band is being crossed. The integer m describes which defect state is involved in the intersection, starting with 1 assigned to the first defect state on the left in Figure 5.5. This integer also describes the mode of the defect state within the defect cavity, which does not change across intersections. This equation accounts for why there are more visible anti-crossings in the third band than there are in the second band in Figure 5.5. The higher j value of the third band leads to more frequent defect sizes t_d such that the defect state is in resonance with the band.

We have established that the states within a multi-cavity device can be split into defect states and band states. The defect states act mostly like isolated single-cavity states except when they are at such a wavelength that they are on resonance with a photonic band. At that point, the defect states cease to be localized to the defect cavity, and a perfect crystal phase is formed with evenly spaced states. As the defect grows beyond a perfect crystal state, a new defect state is formed from the highest wavelength state in the band, and that state begins to act like a single-cavity state once again. The behavior of the bands requires more work to fully understand.

Chapter 6

Band Behavior in Devices with Defects

We have observed that when one cavity in a three-cavity device has a defect, two of the states from each photonic band remain in that band. However, this does not mean that they are unaffected by the presence of the defect cavity. The primary behavior of the band states in our center-defect device is to collapse onto each other, becoming almost entirely degenerate at the point when the defect state is in the middle of the band gap. The electric field profile of the band states does not shine much light on the roots of this behavior, but we can gain greater insight by looking at the electric field broken down by the cavity in which it is generated.

At a defect cavity size of 128%, the two states in the photonic band appear to have completely collapsed on to one another (see figure 5.4). However, peak-fitting software can identify that the single, lopsided peak we see is comprised of two distinct peaks in the emission of the device. There is the obvious peak at 667 nm, but there is a second, less intense peak at 670 nm as well. Figure 6.1 shows how similar these

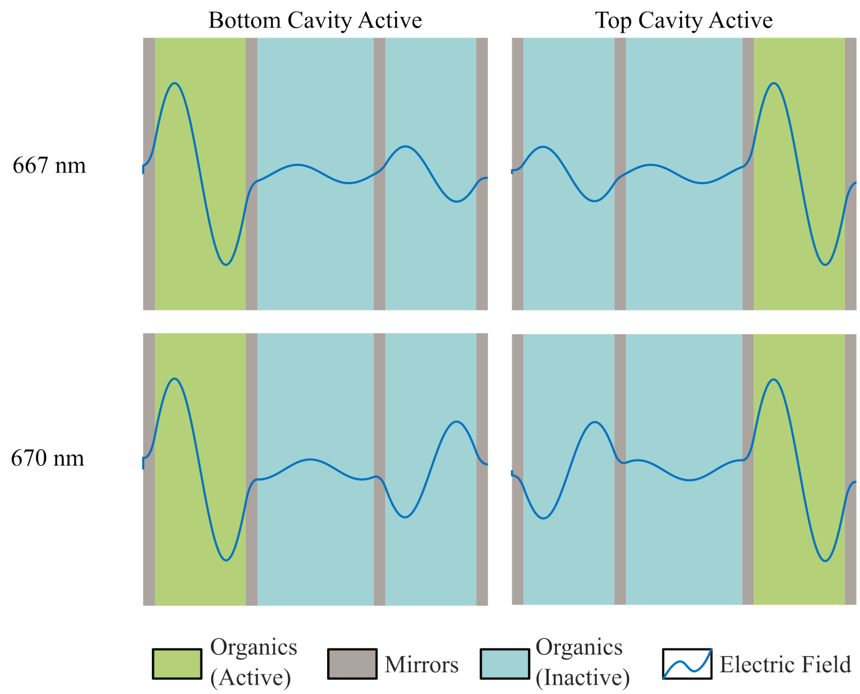

Figure 6.1: Profile of electric field generated in the static cavities of a device with a 128% defect in the center cavity. Shown are the two band states at 667 nm and 670 nm.

two states are, and therefore why they are so difficult to distinguish.

The first remarkable thing about Figure 6.1 is how the field generated in the bottom cavity does not strongly resonate in the top cavity and vice versa. They have the same resonance condition, seeing as they are identical, but it seems that the field generated on one end of the device fails to reach the other end. Evidently, the symmetrical field profile in Figure 5.4 is hiding an underlying truth. The total field is actually the sum of two, almost completely independent states in the top and bottom cavity. Each one does not strongly contribute to the amplitude of the other. Due to the symmetrical nature of the device, these two states are still identical, so they are not distinguishable as two different states in either the total electric field or the emission.

The 670 nm state looks very similar to the more clearly visible 667 nm state. The only difference lies in the very limited waves that each static cavity transmits to the other. While the field generated in the bottom cavity is in phase with the field generated in the top cavity in the 667 nm state, the opposite is true in the 670 nm state. This constructive and destructive interference is what sets these two states apart. It seems natural, then, that when the transmission or communication from one cavity to the other becomes extremely weak, the difference between the two states disappears. The collapse of the two states into one degenerate state comes from the defect cavity disrupting the communication between them.

There are two easy ways to test this theory. We know that when the device is in a perfect crystal phase, all three states are clearly distinct from each other. According to what we've found here, we would predict that while in that phase, the top and bottom cavities are able to communicate with each other and that the field generated by the bottom cavity resonates strongly in the top cavity. We would also predict, that if the defect cavity were not physically placed between the two static cavities, then the band states would never collapse on each other, and they would remain distinct regardless of the status of the defect cavity. The results of these experiments are shown in Figure 6.2.

In order to block communication between the two static cavities, the defect cavity must be located between them and it must be out of resonance with them. This is why we do not see the band states collapse into degeneracy in Figure 6.3, where the defect is in the top cavity. Instead, following the perfect crystal phase, the two band states return to a greater separation than what they have in the three-state band. Previous work on MDPC OLEDs suggests that band width does not depend

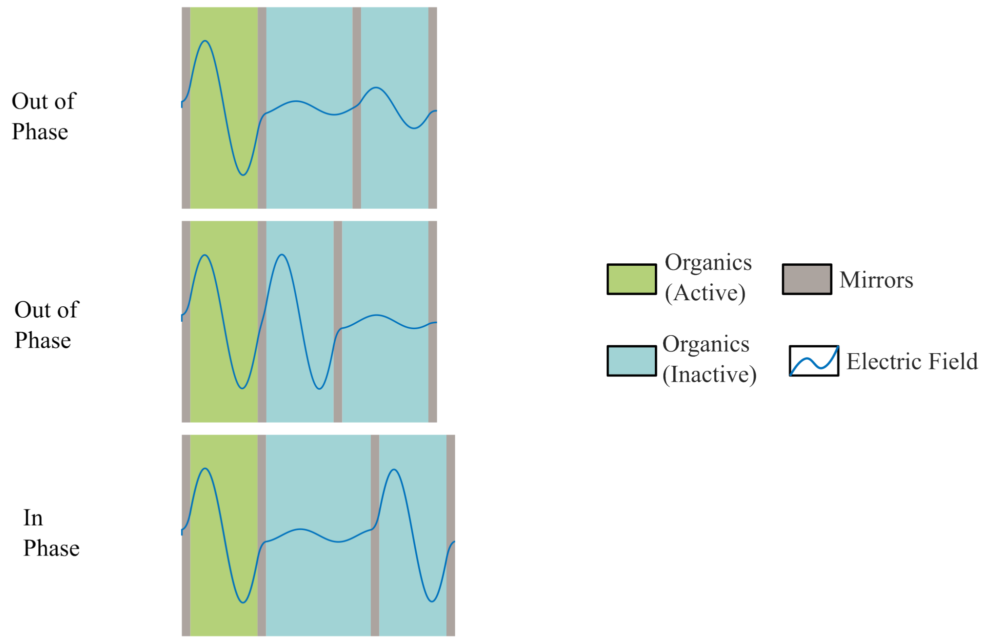

Figure 6.2: Profiles of electric field generated by the bottom cavity with different defect size and position

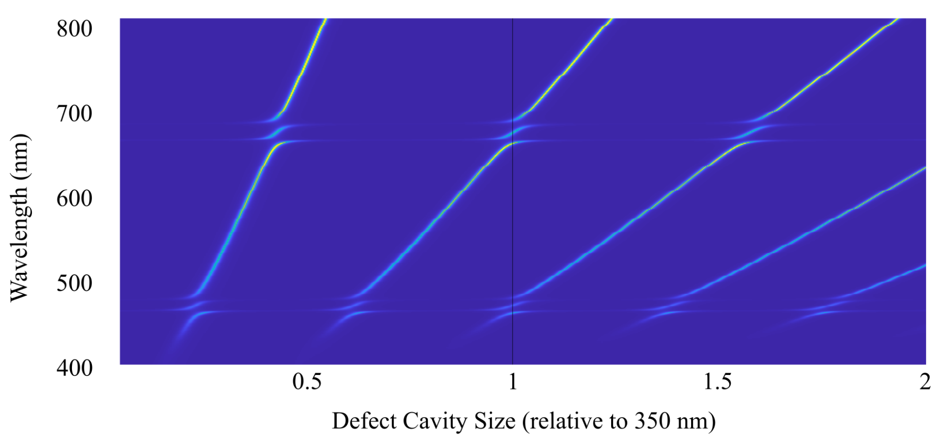

Figure 6.3: Emission from devices with a wide range of defects on the top cavity. Defect cavity size is represented as a fraction of 350 nm.

strongly on number of cavities, so the two state band will naturally have wider state spacing than the three-state band [10]. Defect location becomes an interesting degree of freedom in any device design and production in the future. When creating a device with a single state in the band gap, we can choose to maintain the structure of the remaining band, by placing the defect on the top or bottom cavity, or we can disrupt the band structure by placing the defect in the middle of the static cavities.

Chapter 7

Larger Crystals and Multiple Defects

The theory we have laid out in the last few chapters lays the groundwork for predicting and explaining the behavior of arbitrarily large devices that may include any number of defect cavities. The introduction of a defect into one cavity in a MDPC OLED leads to the creation of a defect state in the band gap. That state will decouple from the states in the band and will grow with the defect size as an isolated single cavity state. When the peak wavelength of the defect state matches the peak wavelength of another band, the defect state will delocalize and become a band state. The separation of distinct states from within a band comes from the interaction, meaning constructive or destructive interference, between the electric field standing waves generated by two or more cavities. If two or more cavities cannot strongly transmit electric field to each other, they will decouple, causing the collapse of distinct band states into a single degenerate state. We found that one can block communication between two cavities by placing a cavity between them that is out of resonance with them.

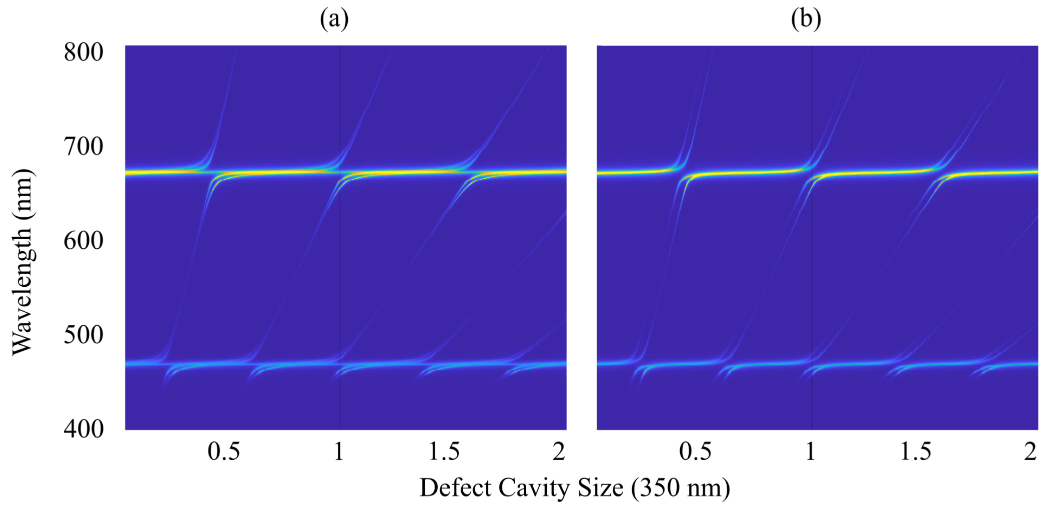

Figure 7.1: (a) A five-cavity device with defects in the second and fourth cavities. The band states collapse because there are no adjacent static cavities and the defect states collapse because there are no adjacent defect cavities. (b) A four-cavity device with defects in the second and third cavities. The defect states maintain their spacing because the defect cavities are adjacent. The band states collapse because the static cavities are separated by defect cavities

Using all of this information, we can make predictions like: a five-cavity MDPC OLED with defects in the second and fourth cavity will have a photonic band of three static states that collapse into one degenerate state and two defect states that collapse into one, except when the whole thing is in resonance, where there will be five evenly spaced states in the photonic band. Likewise, a four-cavity device with two defect states in the center cavities will have its two band states collapse into one, but the defect states will always maintain their spacing because they are directly adjacent. The two experiments described here are shown in Figure 7.1.

The more complex configurations still follow the fundamental rules of our theory, but the results still may not be intuitive. For example, the case of a five-cavity device with a single defect in the center cavity leads to a 4-state band that collapses not

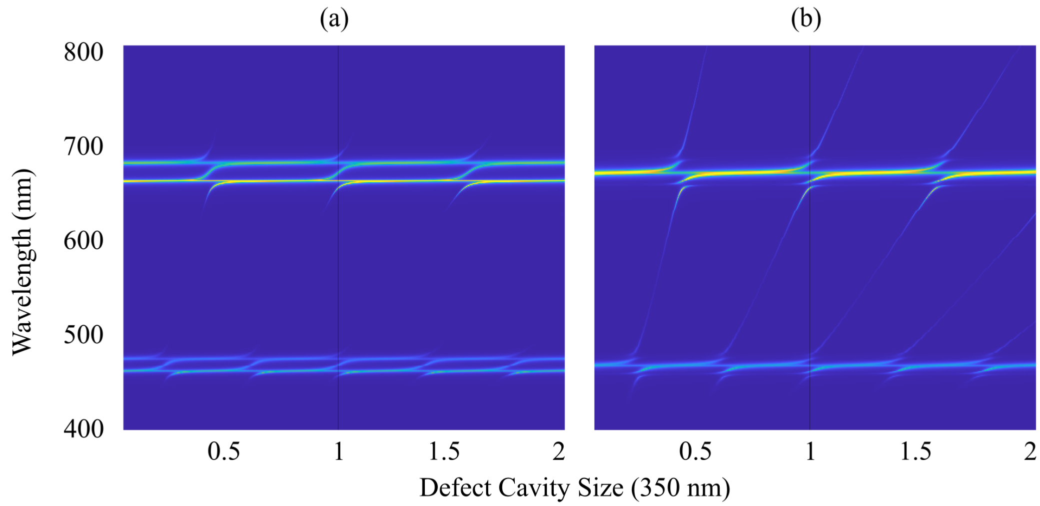

Figure 7.2: (a) A five-cavity device with a defect in the center cavity. Two independent two-state bands are formed and collapse together into a degenerate two-state band. (b) A five-cavity device with a defect in the fourth cavity. The isolated state generated in the top cavity is degenerate with the center state of the three-state band

into one state, but into two degenerate states. The same two states are generated by the top and bottom pairs of cavities, so they collapse such that those two states are distinct, but the band generated in the top pair is indistinguishable from the band generated in the bottom pair. If we move the defect to the fourth cavity, then we get a set of cavities forming a three-state band, and a single cavity that is not part of that band. The single state overlaps with the center state of the band, creating a band with one degenerate band state and two normal band states. The results of these defects can be seen in Figure 7.2.

These figures start to show some behavior that is as unfortunate as it is predictable. We have already shown that if a cavity is resonating at a certain wavelength, it will not transmit well through a cavity with a different resonant wavelength. This means that, as is the case in Figure 7.2 (a), if there are multiple static cavities between the defect cavity and the top of the device (where emission is viewed), the defect state will not out-couple well, and in some cases may not be visible. Similarly, in Figure 7.2 (b), the band states that are formed in the three bottom cavities can be quite faint due to the fact that there is a defect cavity between them and the out-coupling layer.

When viewing Figure 7.2 (b) and applying the reasoning we have developed, it is tempting to think that the isolated state generated in the top cavity of the device is completely constant. It appears not to shift near the crystal phase the way the other states do, and it is not part of any band. However, if you look closely, the line that, at one intersection, represents the isolated cavity state actually shifts upwards at the next intersection to become the lowest wavelength state in the three-state band, and that same line will shift again at the following intersection to become the new defect state. This happens because our description depends on certain states being isolated to single cavities. While this is a good description outside of the crystal phase, we know that all the states become spatially extended across the entire device any time the defect states are in resonance with the band states. When the defect moves out of resonance, and the states become localized again, it is not necessary for a certain state to be localized to the same cavity it was in before. In some ways, this can be seen as a failure of our model - our description fundamentally splits the behavior into two distinct regimes. It is possible to create a description that does not rely on phase changes, but this description comes with its own drawbacks as well.

Chapter 8

Perturbed Harmonic States - A Thin Mirror Approach to Describing Defect States

The approach that has been used so far to explain the behavior of defected MDPC OLEDs is based on the "coupled oscillator" model. This model provides significant insight and accurately predicts the behavior of defected devices, particularly when the defected cavity is out of resonance with the static cavities, and when the mirrors between devices are relatively thick. A shortcoming of this description is that it requires us to divide the behavior of our devices into two regimes: out-of-phase defects and in-phase defects. There is a second description of MDPC OLEDs, which is most applicable when the mirrors in a device are relatively thin, and that is the "perturbed harmonic state" model. This model, described by Figure 3.4, does not rely on the idea of localized states [10]. Instead, each state is described as a perturbed version of the harmonic states that would naturally resonate in the device if it had no internal

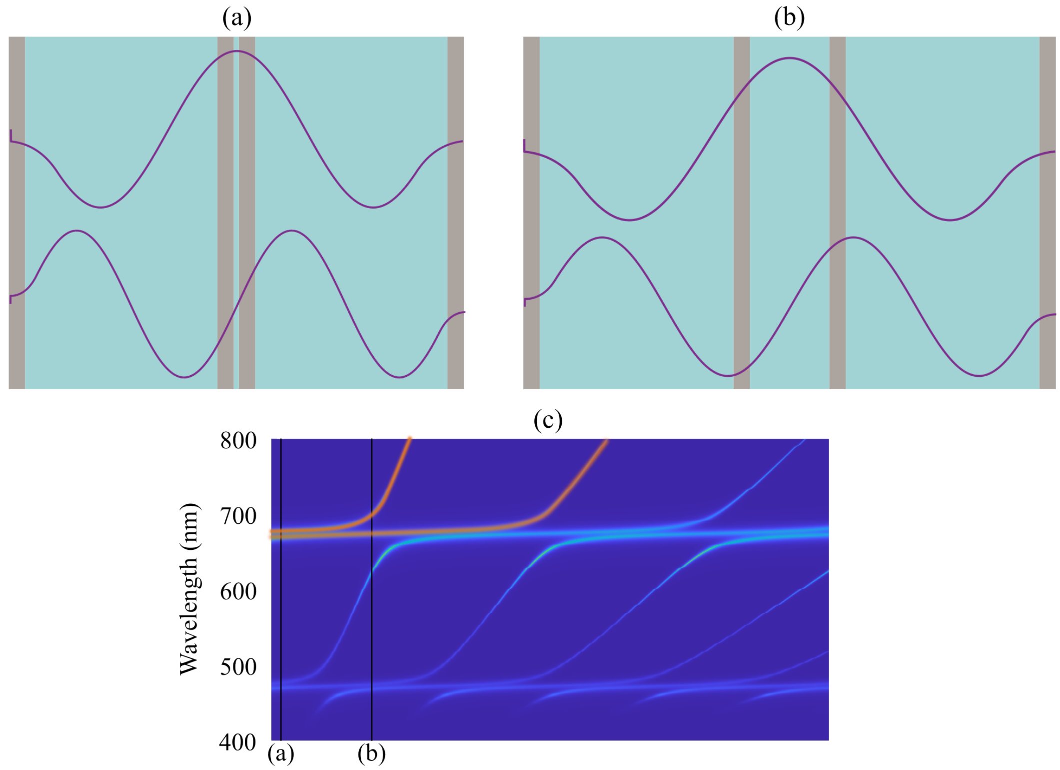

Figure 8.1: The perturbation of harmonic modes in defected devices with 30nm mirrors. (a) and (b) show the mirror positions of devices with defect cavity sizes of 0.05 and 0.35 respectively, overlaid with the unperturbed third and fourth harmonic modes. The effects of the perturbation are shown in (c), with the relevant states highlighted in red

mirrors. The mirrors perturb the harmonic states, particularly when they fall on anti-nodes. This perturbation causes the wavelength of the state to decrease, and this effect combines with the natural pattern of the harmonic modes to create bands of states.

This theory of perturbation can be applied to defected MDPC OLEDs just as well, bearing in mind that the greatest perturbation will occur when the mirrors fall on anti-nodes of the harmonic states and that perturbation causes the wavelength of a state to decrease. An advantage of this model is that each of the long, continuous curves seen in figures like Figure 5.2 is assigned to a harmonic, and we do not need to make arguments about how delocalization causes states to jump from one line to another. In this way, we have eliminated the idea that there are separate regimes to consider, and this description works equally well for any defect size.

Figure 8.1 shows how the changing levels of perturbation affect the third and fourth harmonic of a defected device. Starting from the case of an extremely small defect cavity, we can see in 8.1(a) that the third harmonic will have maximum perturbation because the two mirrors fall very close to the central anti-node of the unperturbed standing wave. As the defect cavity grows, the amount of perturbation decreases while the overall device size increases. Both of these effects work to increase the wavelength of this state, leading to the significant change seen in 8.1(b) where the perturbation is much less because the mirrors are nearly in the position of the third harmonic's nodes.

The fourth harmonic has the opposite experience. This state is in a perturbation minimum in Figure 8.1(a) and the growing defect cavity can only increase the amount of perturbation the standing wave will experience, driving the wavelength of the state down. This effect is in opposition to the effect of the lengthening cavity, and the two very nearly cancel out. This state will remain at the same wavelength through 8.1(b) until a defect size of nearly 1.0, at which point the mirrors will pass by the standing wave's central anti-nodes and the magnitude of perturbation will fall, causing the inflection of this curve seen just left of center in Figure 8.1(c).

The sixth harmonic can be seen at the beginning of a period of wavelength stagnation in Figure 8.2. As described above, this transition occurs when the standing wave has reached a perturbation minimum, so that the magnitude of perturbation can only increase as the defect cavity grows. The fact that an anti-crossing always occurs

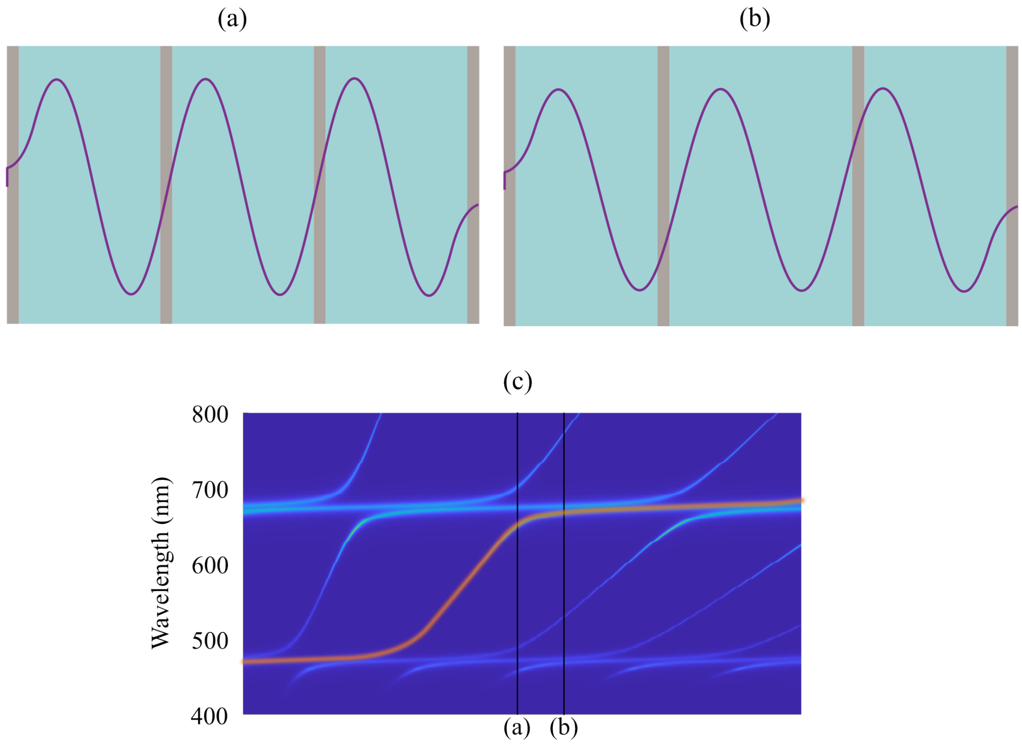

Figure 8.2: The perturbation of harmonic modes in defected devices with 30nm mirrors. (a) and (b) show the mirror positions of devices with defect cavity sizes of 1.0 and 1.15 respectively, overlaid with the unperturbed sixth harmonic mode. The effects of the perturbation are shown in (c), with the relevant state highlighted in red

when one state has mirrors at its nodes serves to explain why the lower-wavelength bands have more frequent anti-crossings. We expect the frequency of anti-crossings to be proportional to the number of anti-nodes that a given state has.

We know the end-behavior of any given state is to pass a final anti-crossing and then increase in wavelength without bound. In our "coupled oscillators" model, we explained this as a given defect state never again resonating with the states in the static cavities. In the "perturbed harmonic states" model, this behavior comes when the internal mirrors pass by the outermost anti-nodes of a given harmonic. Beyond this point, a larger defect cavity can only decrease the perturbation of the standing

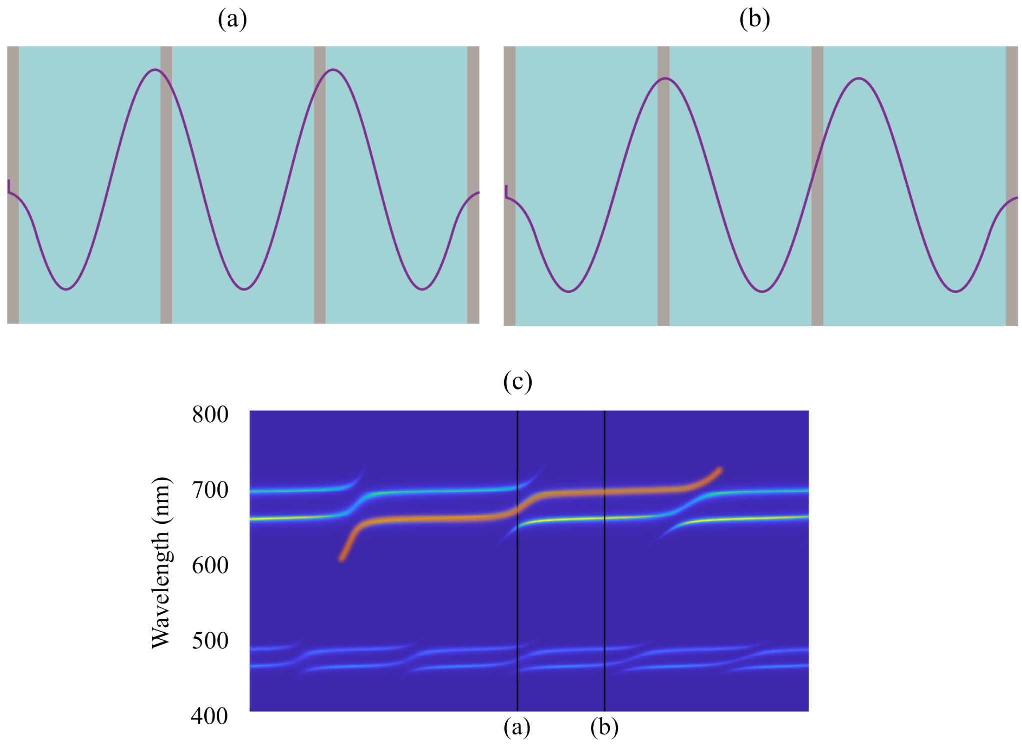

Figure 8.3: The perturbation of harmonic modes in defected devices with 30nm mirrors. (a) and (b) show the mirror positions of devices with top-position defect cavity sizes of 1.0 and 1.25 respectively, overlaid with the unperturbed fifth harmonic mode. The effects of the perturbation are shown in (c), with the relevant state highlighted in red

wave, and the wavelength of the state will be governed primarily by the growing size of the device as a whole.

A disadvantage of this model is that it does not easily handle the displacement of the defect to the top cavity. When the device is symmetrical, the internal mirrors reach nodes and anti-nodes simultaneously, and the perturbation created by each one always matches the other. However, when the defect creates asymmetry in the device, the internal mirrors will reach nodes and anti-nodes at different defect sizes, leading to more complex behavior.

The fifth harmonic, located in the center of the second band, has a brief period of wavelength growth centered around a defect cavity size of 1.0. The cause for this small-scale increase is shown in Figure 8.3. Near this defect cavity size, the two mirrors pass over two anti-nodes at different times, leading to two distinct regions of high perturbation. Between these two, there is a local perturbation minimum from defect sizes of about 0.95 to 1.05. While at this minimum, the increasing size of the device causes the state to grow in wavelength, before it is suppressed again by the perturbation caused by the second mirror reaching an anti-node.

In this manner, any defect size or arrangement can be analyzed and explained. The coupled oscillator model also has the advantage of being more directly quantifiable, while perturbations of the harmonic modes remain qualitative. As is the case in MDPC OLEDs without defects, the reality of a given device lies between the two extremes proposed by these thin- and thick-mirror approximations, and each serves in its way to explain the whole.

Chapter 9

Conclusions

The behavior of Metal-Dielectric Photonic Crystal OLEDs with one or more defect cavities can be described in terms of either of the two models that are applied to MDPC OLEDs in general, provided appropriate adjustments are made to account for the asymmetry of the cavities. The first model suggests that each cavity be treated as a distinct resonator, and that the overall behavior can then be found by allowing the cavities to couple to their neighbors. The second model is based on the standing waves that exist in a large cavity with no internal mirrors. The behavior of an MDPC OLED can be found by considering the perturbations in these waves created by introducing thin mirrors at given locations. Any fully symmetrical MDPC OLED can be described as being in an intermediate state between these two extremes, given the dimensions of the metal and dielectric layers. Applying either model will generate the photonic band structures that are characteristic of MDPC OLEDs.

The perturbed harmonic description changes very little upon in the case where dielectric layers can have different dimensions. The peak emission wavelengths can still be qualitatively predicted by approximating the level of perturbation caused by the location of the mirrors relative to the nodes and anti-nodes of a given standing wave. These predictions may be tedious and imprecise, given that mirror position in an asymmetrical device is not intuitive, and as yet there is not a method for quantifying perturbation.

When applying the coupled oscillator model to an MDPC OLED device that does not have identical cavities, the only adjustment that must be made is that the cavities have different characteristic wavelengths and frequencies. The band structures can still be predicted by considering each uninterrupted block of identical cavities. Each block will form its own band, and cavities that are not part of a block will generate peaks based solely on their optical path length.

This work could be adapted from the realm of simulation to theory by applying mathematically rigorous models for coupled oscillators to the MDPC OLED system. In classical physics, normal mode frequencies can be found based on the natural frequency of each oscillator and a coupling parameter. We know already the natural frequency of each of our oscillators, based on its optical path length and the penetration depth into the mirrors. The coupling parameter for adjacent cavities should depend on the physical characteristics of the mirror between them, and a working model that described this parameter would allow for a very rigorous description of the states generated by any MDPC OLED.

Bibliography

[1] Yu Chen, Xining Zang, Jiajun Gu, Shenmin Zhu, Huilan Su, Di Zhang, Xiaobin Hu, Qinglei Liu, Wang Zhang, and Dingxin Liu. Zno single butterfly wing scales: synthesis and spatial optical anisotropy. *J. Mater. Chem.*, 21:6140–6143, 2011.

[2] Dorota A Pawlak. Metamaterials and photonic crystals–potential applications for self-organized eutectic micro-and nanostructures. *Scientia Plena*, 4(1), 2008.

[3] John D Joannopoulos, Pierre R Villeneuve, and Shanhui Fan. Photonic crystals: putting a new twist on light. *Nature*, 386(6621):143–149, 1997.

[4] Jean Pol Vigneron and Priscilla Simonis. Natural photonic crystals. *Physica B: Condensed Matter*, 407(20):4032–4036, 2012.

[5] Zofia Vértesy, Zs Bálint, K Kertész, JP Vigneron, V Lousse, and LP Biró. Wing scale microstructures and nanostructures in butterflies- natural photonic crystals. *Journal of microscopy*, 224(1):108–110, 2006.

[6] C J R Sheppard. Approximate calculation of the reflection coefficient from a stratified medium. *Pure and Applied Optics: Journal of the European Optical Society Part A*, 4(5):665, sep 1995.

[7] Eli Yablonovitch. Photonic crystals: semiconductors of light. *Scientific American*, 285(6):46–55, 2001.

[8] Ekraj Dahal, David Allemeier, Benjamin Isenhart, Karen Cianciulli, and Matthew S White. Characterization of higher harmonic modes in fabry–pérot microcavity organic light emitting diodes. *Scientific reports*, 11(1):8456, 2021.

[9] Arafa H Aly, Mohamed Ismaeel, and Ehab Abdel-Rahman. Comparative study of the one dimensional dielectric and metallic photonic crystals. *Scientific Research Optics and Photonics*, 2012.

[10] David Allemeier, Benjamin Isenhart, Ekraj Dahal, Yuki Tsuda, Tsukasa Yoshida, and Matthew S White. Emergence and control of photonic band structure in stacked oled microcavities. *Nature Communications*, 12(1):6111, 2021.

[11] Stefan Kappaun, Christian Slugovc, and Emil JW List. Phosphorescent organic light-emitting devices: working principle and iridium based emitter materials. *International journal of molecular sciences*, 9(8):1527–1547, 2008.

[12] Matthew S White, Martin Kaltenbrunner, Eric D Głowacki, Kateryna Gutnichenko, Gerald Kettlgruber, Ingrid Graz, Safae Aazou, Christoph Ulbricht, Daniel AM Egbe, Matei C Miron, et al. Ultrathin, highly flexible and stretchable pleds. *Nature Photonics*, 7(10):811–816, 2013.

[13] Tsubasa Sasaki, Munehiro Hasegawa, Kaito Inagaki, Hirokazu Ito, Kazuma Suzuki, Taku Oono, Katsuyuki Morii, Takahisa Shimizu, and Hirohiko Fukagawa. Unravelling the electron injection/transport mechanism in organic light-emitting diodes. *Nature Communications*, 12(1):2706, 2021.

[14] LS Hung, Ching Wan Tang, and Monica Gary Mason. Enhanced electron injection in organic electroluminescence devices using an al/lif electrode. *Applied Physics Letters*, 70(2):152–154, 1997.

[15] Martin Knupfer. Exciton binding energies in organic semiconductors. *Applied Physics A*, 77:623–626, 2003.

[16] N Thejo Kalyani and SJ Dhoble. Organic light emitting diodes: Energy saving lighting technologyâa review. *Renewable and Sustainable Energy Reviews*, 16(5):2696–2723, 2012.

[17] Guijiang Zhou, Wai-Yeung Wong, and Si Suo. Recent progress and current challenges in phosphorescent white organic light-emitting diodes (woleds). *Journal of Photochemistry and Photobiology C: Photochemistry Reviews*, 11(4):133–156, 2010.

[18] Miaosheng Wang, Jie Lin, Yu-Che Hsiao, Xingyuan Liu, and Bin Hu. Investigating underlying mechanism in spectral narrowing phenomenon induced by microcavity in organic light emitting diodes. *Nature communications*, 10(1):1614, 2019.

[19] Ananth Dodabalapur, LJ Rothberg, RH Jordan, TM Miller, RE Slusher, and Julia M Phillips. Physics and applications of organic microcavity light emitting diodes. *Journal of applied physics*, 80(12):6954–6964, 1996.

[20] Chih-Hao Chang, Hsing-Chieh Cheng, Yin-Jui Lu, Kun-Cheng Tien, Hao-Wu Lin, Chun-Liang Lin, Chih-Jen Yang, and Chung-Chih Wu. Enhancing color gamut of white oled displays by using microcavity green pixels. *Organic Electronics*, 11(2):247–254, 2010.

[21] Meera M Parish. Excitons in a new light. *Nature Physics*, 17(1):16–17, 2021.

[22] David Allemeier, Nicholas Sobolew, Sean Magnifico, Katherine Henry, Edward Abua, and Matthew S White. High symmetry metal-dielectric photonic crystal organic light emitting diodes with single-cavity unit cells. *Advanced Optical Materials*, 11(2):2201631, 2023.